Nuclear Materials and Energy 19 (2019) 458–462

Contents lists available at ScienceDirect

Nuclear Materials and Energy

journal homepage: www.elsevier.com/locate/nme

Investigation of recombination front region in detached plasmas in a linear divertor plasma simulator

N. Ohno[a,*], M. Seki[a], H. Ohshima[a], H. Tanaka[a], S. Kajita[b], Y. Hayashi[c], H. Natsume[a], H. Takano[a], I. Saeki[a], M. Yoshikawa[d], H. van der Meiden[e]

[a] Graduate School of Engineering, Nagoya University, Chikusa-ku, Nagoya 464-8603, Japan
[b] Institute of Materials and Systems for Sustainability, Nagoya University, Chikusa-ku, Nagoya 464-8603, Japan
[c] National Institute for Fusion Science, 322-6 Oroshi-cho, Toki, Gifu 509-5292, Japan
[d] Plasma Research Center, University of Tsukuba, 1-1-1 Tennodai, Tsukuba 305-8577, Japan
[e] DIFFER – Dutch Institute for Fundamental Energy Research, De Zaale 20, 5612 AJ Eindhoven, the Netherlands

ARTICLE INFO

Keywords:
Divertor
Detached plasma
Volume recombination
Recombination front

ABSTRACT

We have investigated detailed plasma structure around the recombination front region (RFR), where volume electron-ion recombination (EIR) strongly occurs in detached plasmas, by using two-dimensional (2D) movable probe system as well as laser Thomson scattering diagnostics. The 2D distribution of electron density, electron temperature, and plasma potential around the RFR, has been revealed for the first time. The spatial distribution of the particle loss rate due to EIR estimated from electron temperature and electron density profiles indicated that the three-dimensional structure of the RFR adopts a cone structure. Furthermore, in the peripheral region of the RFR, the radial profile of the electron density was widened locally with increasing cross-field transport caused by plasma fluctuation. From the heat transport analysis of electrons, it was found that the thermal relaxation process between electrons and ions is important for the cooling of electrons, and that the convection of electrons regulates electron heat transport near the RFR.

1. Introduction

Reducing particle and heat flux onto a divertor plate using plasma detachment is the most important issue in nuclear fusion research [1]. The footprint profile of particle and heat flux on the divertor plate broadens associated with volume electron-ion recombination and enhancement of cross-field transport in detached plasmas. Divertor probe measurement in the TdeV tokamak shows that a radial profile of ion flux to the divertor plate broadens due to plasma detachment [2]. In the LHD device, broadening of the ion flux profile toward the low field side was observed accompanied with plasma fluctuation in the detached plasma condition [3]. An important question is where the plasma distribution becomes broader in the detached divertor regions.

In the plasma detachment, electron temperature T_e decreases to be 5 eV along magnetic field lines, because electrons are cooled down due to electron impact excitation and ionization process in the upstream region. When T_e reaches below 1 eV with high plasma density, electron–ion recombination (EIR) occurs to reduce particle and heat flux to the divertor plate. The region, where EIR occurs strongly, is referred to as “recombination front region (RFR)”. The structure and dynamic behavior of the RFR determine the footprint profile on the divertor plate. Therefore, it is very important to reveal the structure and behavior of the RFR in detached plasmas.

Linear divertor plasma simulators have been widely utilized to investigate plasma detachment phenomena [4], because they can generate steady-state detached plasmas by controlling plasma-gas interaction with a simple geometrical configuration. Axial profiles of the RFR have been investigated with Langmuir probe and spectroscopy in the linear devices. Axial profiles of Hα emission were measured with spatially resolved spectroscopy as a parameter of hydrogen neutral pressure in the ULS [5]. Concerning an axial plasma potential profile, the PDS device showed an electrostatic potential double layer structure, formed near the RFR [6]. The formation of the double layer could be related to stability of detached plasma. Further investigation of the RFR, located near the boundary between attached and detached plasmas, should be required. However, there have been few studies on 2D plasma structure near the RFR.

In this study, we have measured detailed 2D plasma profiles near RFR in detached plasmas for the first time to investigate particle and heat transport in the RFR.

* Corresponding author.
E-mail address: ohno@ees.nagoya-u.ac.jp (N. Ohno).

https://doi.org/10.1016/j.nme.2019.03.010
Received 14 August 2018; Received in revised form 14 February 2019; Accepted 6 March 2019
Available online 05 April 2019

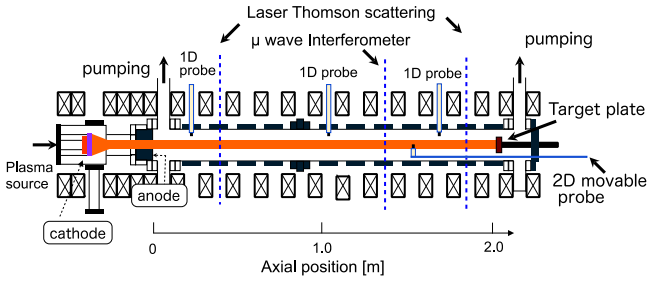

Fig. 1. Schematic view of the linear divertor plasma simulator, NAGDIS-II.

2. Experiments

Experiments have been conducted by utilizing a linear plasma device NAGDIS-II [7] shown in Fig. 1. The NAGDIS-II can generate a high-density plasma above 10^{19} m^{-3} by a dc discharge with a 109 mm diameter disk LaB_6 cathode and a copper hollow anode of 24 mm in a diameter. The radius of the plasma column defined by the half maximum width is about 20 mm, determined by a diameter of the hollow anode. The working gas of helium (He) was injected to plasma source region, and pumped out by two turbomolecular pumps (2000 L/s and 2400 L/s) located at upstream and downstream. The generated He plasma in the plasma source was introduced into plasma test region along magnetic field lines and finally terminated by a target plate at an axial position of 2.05 m. The strength of the magnetic field was 0.1 T.

The NAGDIS-II has several diagnostic systems. Three fast-reciprocating Langmuir probes were installed to measure radial profiles of electron density and temperature at different axial positions. Two laser Thomson scattering (LTS) systems were installed at axial positions of 0.4 m and 1.88 m. The second harmonics laser beam (wavelength of 532 nm) of an Nd:YAG laser device was utilized with a pulse width of 5–10 ns, the pulse energy of ~0.3 mJ and a repetition rate of 10 Hz. The collected scatter light was transferred through the optical fiber, which has 23 channels, to the spectrometer with Gen-III ICCD camera. The LTS system, improved by the international collaboration with DIFFER in the Netherlands, makes it possible to measure electron density and temperature less than 1 eV in detached plasmas [8,9]. A microwave interferometer with a frequency of 70 GHz developed by Univ. of Tsukuba was installed to measure plasma density fluctuation [10]. The emission intensity of visible light from plasma can be measured through viewports located on the side of the device.

To measure two-dimensional (2D) structure of RFR, we have newly developed 2D movable Langmuir probe system (2D LP). The axial position of the probe was controlled by a computer-aided linear actuator. Further, the probe head can be rotated in the radial direction to obtain 2D plasma profiles. The probe measurement system has been improved based on the LTS data.

Neutral He pressure was measured with a MKS Baratron Capacitance Manometer. The ionization mean free path of He atom is longer than the diameter of plasma column (20 mm). Therefore, the neutral He pressure in plasma column is almost equal to that outside the plasma column.

3. Experimental results

Feeding additional He gas from the inlet at the end of the device to increase neutral He pressure can produce detached He plasmas. Fig. 2(b)–(d) show typical photos indicating the transition from attached to detached plasmas in the NAGDIS-II. Fig. 2(b) shows ionizing plasma column on the upstream side. The plasma color was orange. In the downstream side, the plasma color changed to purple, associated with EIR, and the light emission distribution became broader in the radial direction shown in Fig. 2(c). Finally, the plasma disappeared near the target plate shown in Fig. 2(d). Fig. 2(a) shows an axial profile of

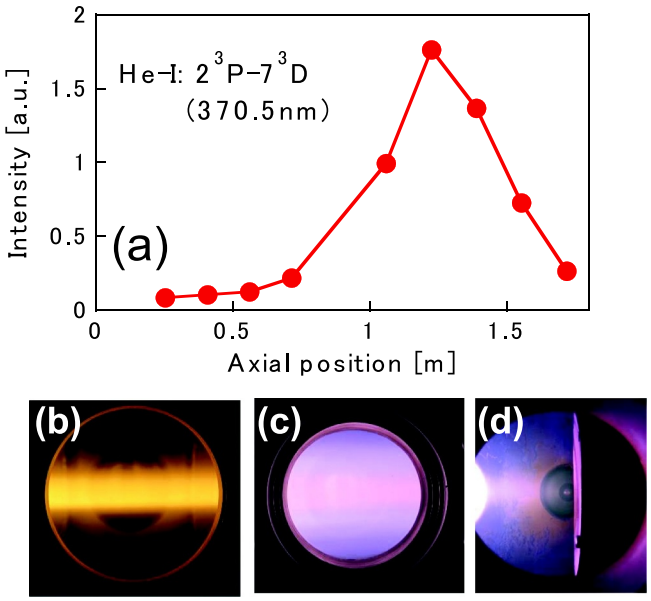

Fig. 2. (a) Axial intensity profile of visible line emission (HeI:2^3P-7^3D, wavelength: 370.5 nm) (b)–(d): photos of detached plasmas taken at upstream, downstream, and near the target plate.

the visible light emission (HeI: 2^3P-7^3D, wavelength: 370.5 nm) intensity at a neutral He pressure of 3.0 Pa. The line emission is attributed to highly excited state of He atoms produced by EIR. The emission intensity peaks at the axial position of 1.3 m. In the region where the emission intensity peaks, strong EIR occurs. The hatched region with large emission intensities is defined as a recombination front region (RFR). The axial position of the RFR can be controlled by controlling the additional He gas flow rate.

By reducing the neutral He pressure to 1.32 Pa, the axial position of the RFR was controlled to be set around 1.7 m in order to measure plasma parameters near the RFR by using the 2D LP. Fig. 3 shows the axial distributions of electron density n_e, electron temperature T_e, and plasma pressure P measured using the 2D LP. The plasma pressure P is a static pressure without dynamic component, which is estimated by the product of n_e and T_e. It can be seen that n_e slowly decreases initially in the upstream and drops sharply in the RFR. On the other hand, T_e starts to decrease at the upstream of the RFR and drops below 1 eV in the RFR. At T_e below 5 eV, electrons cannot be cooled down by electron impact excitation and ionization process, because their rate coefficients are quite small. The possible mechanism of cooling electrons would be

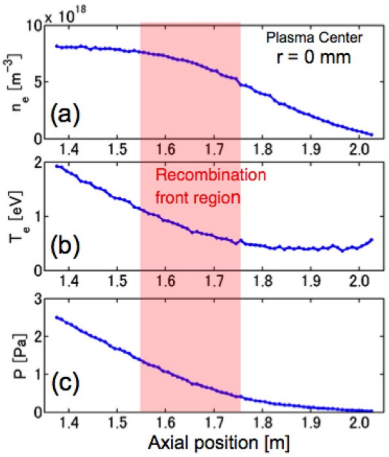

Fig. 3. Axial profiles of (a) electron density, (b) electron temperature, and (c) plasma pressure at the center of plasma column.

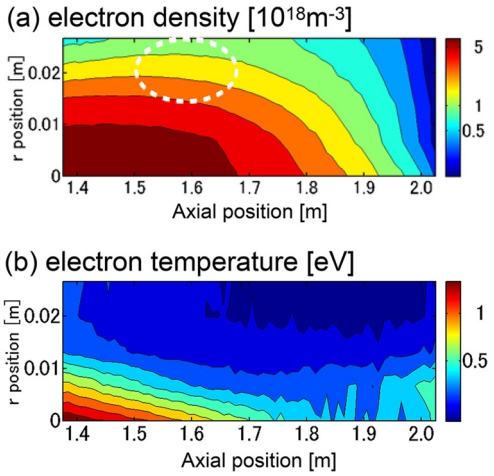

Fig. 4. Two dimensional distributions of (a) electron density, and (b) electron temperature.

thermalization process between electrons and ions, followed by a charge exchange process between ions and atoms.

Fig. 4 shows the 2D distributions of n_e and T_e logarithmically displayed. In the upstream of the RFR, the radial distribution of n_e hardly changes. As the plasma passes through the RFR, n_e at the center of the plasma column sharply decreases, and the radial distribution of n_e flattens. More carefully, it is observed that the radial distribution of n_e is locally spreading at the periphery of the plasma column at the axial position around 1.6 m (the region surrounded by the dotted line) as shown in Fig. 4(a). This experimental result suggests that the cross-field plasma transport locally enhances in the RFR. From T_e distribution in Fig. 4(b), it can be found that T_e decreases monotonically in all radial positions. Further, at the radial position less than 15 mm, the isothermal line of T_e becomes straight, because the decay rate of T_e in the axial direction is almost constant. Therefore, three-dimensionally, the isothermal plane of T_e assumes a cone-like structure.

Based on the 2D distribution of n_e and T_e, the 2D distribution of the particle loss rate S_{rec} [$m^{-3}s^{-1}$] by EIR was estimated. S_{rec} is determined by $\langle\sigma v\rangle_{rec} n_e^2$, where $\langle\sigma v\rangle_{rec}$ [m^3s^{-1}] is the rate coefficient of EIR process. $\langle\sigma v\rangle_{rec}$ was calculated by using collisional-radiative model [11], as shown in Fig. 5(a). $\langle\sigma v\rangle_{rec}$ has a very strong electron temperature dependence; especially, $\langle\sigma v\rangle_{rec}$ becomes quite large at low T_e less than 1 eV. $\langle\sigma v\rangle_{rec}$ also has electron density dependence; larger n_e leads to

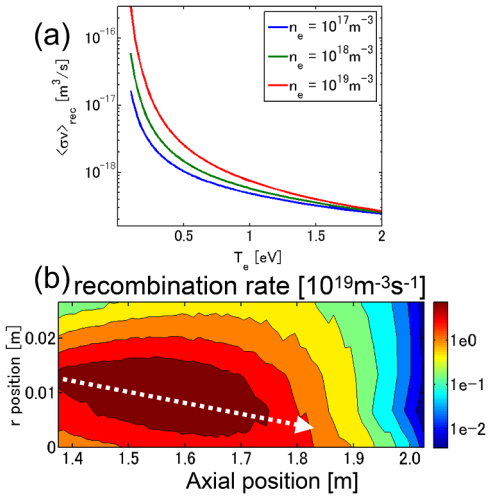

Fig. 5. (a) Rate coefficient of EIR process calculated by using collisional-radiative model, (b) Two-dimensional distribution of particle loss rate (recombination rate) calculated based on Fig. 4.

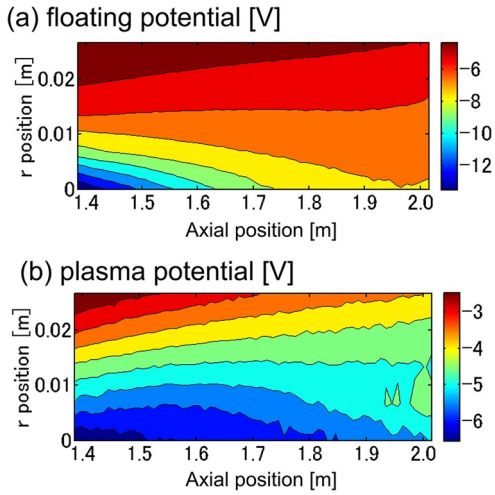

Fig. 6. Two dimensional distributions of (a) floating potential and (b) plasma potential.

larger $\langle\sigma v\rangle_{rec}$. Fig. 5(b) shows the 2D distribution of S_{rec} calculated based on $\langle\sigma v\rangle_{rec}$ and the 2D distribution of n_e and T_e shown in Fig. 4. On the upstream side, the particle loss occurs due to EIR at the periphery of the plasma column (r position of 10 mm), where T_e is about 0.5 eV or less, and n_e is about 5×10^{18} m^{-3}. As the plasma is transported to the downstream side along magnetic field lines, the region with low T_e moves to the plasma center (Fig. 4(b)). On the other hand, since radial n_e distribution does not change so much (Fig. 4(a)), the large particle loss region shifts to the center of the plasma column according to the variation of the T_e distribution, as indicated by the dashed arrow in the figure. Therefore, the structure of the region where the particle loss due to EIR is large, that is, the structure of the RFR takes a cone structure. Unfortunately, in the NAGDIS-II device, it was not possible to visibly measure the cone structure of the RFR due to the limitation of the size and the number of the viewports. However, in the experiment of the linear device MAP-II, the three-dimensional cone-like structure of the RFR was clearly observed [12].

Fig. 6 shows the 2D distributions of floating potential V_f and plasma potential V_p, which was estimated by the following formula: $V_p = V_f + \alpha T_e/e$. The numerical factor α was determined by the floating voltage ϕ described by the following equation:

$$\frac{e\phi}{T_e} = \frac{1}{2}\ln\left[\left(2\pi\frac{m_e}{m_i}\right)\left(1+\frac{T_i}{T_e}\right)\right] = -3.2,$$

where $T_e = T_i$ and m_i is helium ion mass. We also consider the effective potential drop ϕ_{pre} in pre-sheath region, described by $e\phi_{pre}/T_e = -0.5$. Then, we can obtain the formula: $V_p = V_f + 3.7\ T_e/e$. On the upstream side, the radial distribution of V_p has a well structure in which V_p at the plasma center is minimum. The well structure of the V_p in the radial direction is determined by the configuration of the cathode and the hollow anode. In the downstream side, the radial V_p distribution becomes flattened toward the target plate. It is found that in the peripheral region of the plasma column (r position $>$ 5 mm), the plasma potential V_p monotonically decreases along magnetic field lines. On the other hand, in the central region, the well structure of V_p was produced along magnetic field lines. The similar potential well was observed in the detached plasma of the PDS device [6], although the plasma condition was quite different. This potential well would limit the axial transport of low temperature electrons to upstream region, contributing to the enhancement of EIR.

Fig. 7 shows frequency analysis of fluctuation of the ion saturation current I_{sat} measured at each radial position. Near the edge of the plasma column (6.7 and 13.5 mm) at the axial position of ~1.4 m, there is a strong spectral peak at ~24 kHz. This peak could be attributed to

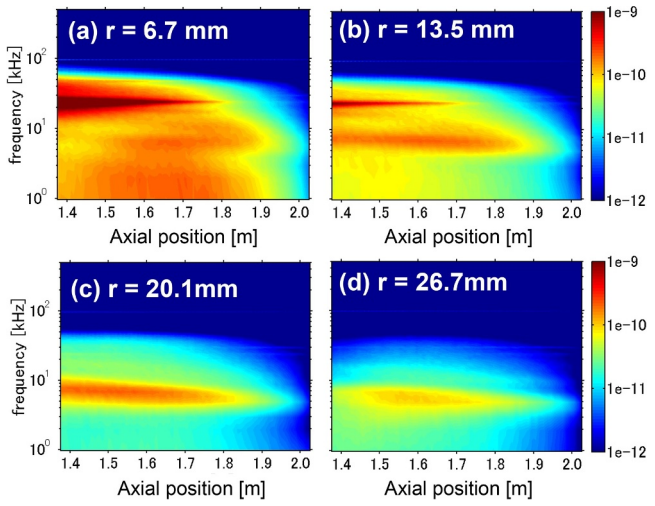

Fig. 7. Dependence of frequency spectra of fluctuation of ion saturation current on axial position at different radial positions (a) 6.7 mm, (b) 13.5 mm, (c) 20.1 mm and (d) 26.7 mm.

the $\boldsymbol{E} \times \boldsymbol{B}$ plasma rotation [13]. On the other hand, in the peripheral region at around the axial position of 1.6 m, I_{sat} fluctuation of 10 kHz or less is appeared and survives at the far peripheral region of $r = 26.7$ mm. This fluctuation could be related to the axially-localized plasma transport propagating toward the radial direction near the RFR.

From the above experimental results, the three-dimensional structure of the RFR was revealed.

4. Discussion

The electron energy loss mainly comes from ionization and radiation when T_e is more than 5 eV. However, at T_e less than 5 eV, electrons cannot lose their energy through the ionization and radiation processes, because the rate coefficient sharply decreases with decrease in T_e. To discuss electron cooling in this electron temperature range, we consider energy transport between electrons, ions and neutrals. Electron and ion thermal equilibration frequency ν_{e-i} is described by $\nu_{e-i} = 3.2 \times 10^{-15} Z^2 \lambda n_e \mu^{-1} T_e^{-3/2}$. λ is the Coulomb logarithm, Z is the ion charge state, and $\mu = m_i/m_p$, where m_p is the proton mass and m_i is the ion mass. Based on the experimental results shown in Fig. 3, ν_{e-i} is calculated to be 108.8 kHz, assuming that $Z = 1$ (singly ionized ions), $\mu = 4$ (He), $\lambda = 17$, $n_e = 8 \times 10^{18}$ m^{-3}, and T_e= 1 eV. Therefore, electron and ion thermal equilibration time $\tau_{e-i} = 1/\nu_{e-i} = 9.2 \times 10^{-6}$ s. The plasma length necessary for thermalization of electrons and ions is estimated by $U_{\text{flow}} \cdot \tau_{e-i}$. The plasma flow velocity U_{flow} is given as $M \cdot C_s$, where C_s is the ion sound velocity and M is the Mach number. We assume $M = 0.5$ near the central region of plasma column, measured in our experiment at a neutral pressure of 1.32 Pa [14]. Therefore, the plasma length is calculated to be 0.032 m, where C_s is 6.9 $\times$ 10^3 m/s for $T_e = T_i$= 1 eV. This calculation indicates that electrons and ions are in thermal equilibrium near the RFR.

He ion energy is dissipated by the charge-exchange process between He ions and atoms because the temperature of He atoms is almost room temperate (0.03 eV). The cross section of the charge-exchange σ_{cx} is about 1.5×10^{-19} m^2, when He ion energy is less than 100 eV [15]. The He atom density $n_n$is estimated to be 2.75 $\times$ 10^{20} m^{-3}, because the natural He pressure is 1.32 Pa and He ion thermal velocity U_i is about 7.8 $\times$ 10^3 m/s for T_i = 1 eV. Therefore, the charge exchange time τ_{cx} can be calculated as follows: $\tau_{cx} = 1/\sigma_{cx}\, n_n\, U_i = 3.1 \times 10^{-6}$ s. It is found that τ_{cx} is smaller than τ_{e-i}, which means that ion energy is rapidly lost due to the charge exchange process. This simple analysis suggests that the electron energy is mainly lost through the ions by the energy exchange between electrons and ions because the ion temperature is kept low due to the charge exchange process with He neutrals.

Next, we would like to discuss the electron heat transport near RFR. The heat conduction of electrons in the direction of the magnetic field lines can be expressed by,

$$q_{cond}^{e} = -3.16 \frac{n_e T_e \tau_e}{m_e} \frac{\partial T_e}{\partial z},$$

where τ_e is electron collision time, described by

$$\tau_e = 3(2\pi)^{3/2} \frac{\varepsilon_0^2 m_e^{1/2} T_e^{3/2}}{n_e e^4 \lambda}.$$

The unit of T_e is [J]. By changing the unit of T_e from [J] to [eV], and assuming $\lambda = 16$, we can derive the following equation.

$$q_{cond}^{e} = -1802\ T_e^{5/2}\ \partial T_e/\partial z\ [\text{W/m}^2].$$

The electron heat transport due to convection, q_{conv}^{e}, can be estimated by $q_{conv}^{e} = 2.5 e T_e n_e\, U_{flow}$. From experimental data around the axial position around 1.5 m shown in Fig. 3(a) and (b), $\partial T_e/\partial z$ = 5 eV/m, T_e = 1.34 eV, and $n_e = 7.9 \times 10^{18}$ m^{-3}, we obtain q_{cond}^{e}=18.7 kW/m^2 and q_{conv}^{e} = 17.2 kW/m^2 by assuming $M = 0.5$. Fig. 8 shows the axial profiles of electron heat flux due to heat conduction and convection at the center of plasma column. It is found that the convection of electrons regulates electron heat transport near the RFR.

5. Summary

In this study, the plasma distribution near the recombination front region of the detached plasma was examined in detail using the 2D probe system. 2D profiles of electron density, electron temperature, plasma potential and particle loss rate near the recombination front region were clarified for the first time. It was found that the electron temperature sharply decreases in the axial direction compared to the electron density. It is also clear that the structure of the iso-electronic-temperature plane has a cone structure. From the 2D distribution of the electron density, the local broadening of the electron density distribution was observed in the peripheral region of the plasma column in the RFR, due to the increase in the local cross-field transport. Furthermore, an axial potential well like electric double layer was observed at the center of plasma column.

Heat transport analysis of electrons was performed based on 2D plasma distribution data. It was shown quantitatively that the thermal relaxation process of electrons and ions and charge exchange process between ions and atoms play an important role in cooling electrons, associated with the charge exchange process between ions and neutrals. Furthermore, near the recombination front region, electron heat convection is dominating.

In the future, we will evaluate effective particle and thermal diffusion coefficients near the RFR by detailed comparison between the experiment results and the 2D fluid code simulation.

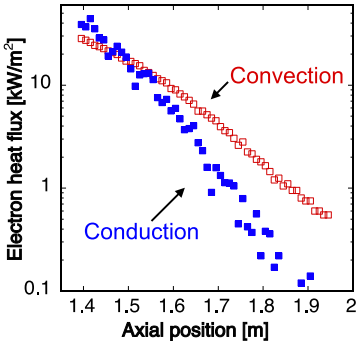

Fig. 8. Axial profiles of electron heat flux due to heat conduction and convection at the center of plasma column.

Acknowledgments

This work was supported by JSPS KAKENHI (16H06139 and 16H02440), the NIFS Collaboration Research program (NIFS16KUGM108 and NIFS17KUGM120), and the NINS program of Promoting Research by Networking among Institutions (01411702).

Supplementary materials

Supplementary material associated with this article can be found, in the online version, at doi:10.1016/j.nme.2019.03.010.

References

[1] G.F. Matthews, J. Nucl. Mater. 220-222 (1995) 104.
[2] B.L. Stansfield, et al., J. Nucl. Mater. 241-243 (1997) 739.
[3] H. Tanaka, et al., Phys. Plasmas 17 (2010) 102509.
[4] N. Ohno, Plasma Phys. Control. Fusion 59 (2017) 034007.
[5] P. Browning, et al., J. Nucl. Mater. 337 (2005) 232.
[6] G. Chiu, S. Cohen, Phys. Rev. Lett. 76 (1996) 1248.
[7] N. Ohno, et al., Nucl. Fusion 41 (2001) 1055.
[8] S. Kajita, et al., Phys. Plasmas 24 (2017) 073301.
[9] H. Ohshima, et al., Plasma Fus. Res. 13 (2018) 1201099.
[10] K. Takeyama, et al., Plasma Fus. Res. 12 (2017) 1202007.
[11] M. Goto, et al., Phys. Plasmas 9 (2002) 4316.
[12] F. Scotti, et al., Plasma Fus. Res. 1 (2006) 054.
[13] H. Tanaka, et al., Plasma Phys. Control. Fusion 60 (2018) 075013.
[14] E.-K. Park, et al., Current Appl. Phys. 12 (2012) 1497.
[15] H.B. Gilbody, J.B. Hasted, Proc. R. Soc. London A 238 (1956) 334.